

Mathematical modeling and simulation of two-phase magnetohydrodynamic flows at low magnetic Reynolds numbers

Jiancheng Wang, Maojun Li, Zeyu Xia, Liwei Xu

School of Mathematical Sciences, University of Electronic Science and Technology of China, Sichuan, 611731, P.R. China

Abstract

We propose a novel mathematical framework for simulating the two-phase incompressible magnetohydrodynamic (MHD) problems. Focusing on low magnetic Reynolds number regimes, where induced magnetic fields are negligible compared to applied fields, an intrinsic sharp-interface system is first formulated. Subsequently, we utilize the phase-field approach to characterize the interface and derive a thermodynamically consistent phase-field model through the Onsager's variational principle. The resulting system couples the Abels–Garcke–Grün (AGG) model of two-phase flows with a quasi-static formulation modeling the electromagnetic phenomena. Theoretically, the sharp-interface limit is investigated via asymptotic arguments, deducing that the sharp-interface system can be recovered in the limit of vanishing interface thickness. Consequently, this justifies the reliability of the phase-field approach as an approximated method. In addition, we present some three-dimensional numerical experiments of magnetic damping effects on bubble dynamics, where the observed results demonstrate the validity of the proposed framework in capturing complex MHD phenomena.

Keywords: incompressible magnetohydrodynamics, two-phase flow, free-interface problem, sharp-interface asymptotics, magnetic damping effect

1. Introduction

When magnetic fields are applied to electrically conducting and nonmagnetic fluids (e.g., liquid metals and strong electrolytes), the induced magnetohydrodynamic (MHD) effects will substantially influence the fluid dynamics, in turn yielding a fundamentally distinct flow behavior. While such phenomena are ubiquitous in industrial processes, problems involving free surfaces (two-phase or free-surface flows) are routinely encountered. Representative examples include continuous casting and refining of metals [11, 23, 40, 43, 55], magnetic destabilization of free surfaces in aluminum reduction cells [7, 19, 28, 48], liquid metal batteries [29, 34, 56, 69], and plasma-facing components [30, 32, 38], among others.

To investigate these intricate MHD behavior, substantial numerical approaches have been developed in the literature. In particular, three established methodologies are typically employed to characterize the interface: volume-of-fluid (VOF) methods [33, 53, 64], level-set (LS) methods [16, 41, 42], and front-tracking (FT) methods [20, 49]. While sharing the same underlying transport equation, VOF methods represent the interface through a volume fraction function, whereas a signed distance function is utilized by LS approaches. In computations, VOF methods require specialized interface reconstruction techniques to maintain interfacial sharpness, and LS methods necessitate periodic re-initialization to preserve numerical stability. On the other hand, FT methods differ fundamentally from VOF and LS approaches through its explicit interface modeling, using either marker particles or an moving interface mesh. This framework offers a precise and direct representation of dynamic interfaces, while demanding frequent mesh regeneration to achieve good mesh quality, particularly during significant interfacial topology changes. Despite their universal employment in two-phase MHD simulations, all three methodologies require considerable numerical efforts to acquire a high-resolution interface [24].

The main purpose of this contribution is to establish a novel mathematical framework for two-phase MHD flows. As our first attempt, we focus exclusively on flows characterized by a magnetic Reynolds number

Email addresses: 202311110403@std.uestc.edu.cn (Jiancheng Wang), limj@uestc.edu.cn (Maojun Li), zeyuxia@uestc.edu.cn (Zeyu Xia), xul@uestc.edu.cn (Liwei Xu)

$Rm \ll 1$, which accounts for most laboratory experiments and industrial processes [12]. The proposed model simultaneously achieves two critical objectives: (i) a precise modeling of complex MHD effects; and (ii) a straightforward formulation for mathematical analysis and numerical implementation. These intrinsic challenges are addressed through a reduced electromagnetic modeling combined with a phase-field (or diffuse-interface) representation for evolving interfaces.

It is well known that electromagnetic fields are governed by pre-Maxwell dynamics in MHD flows; see equations (3). Our reduced electromagnetic formulation is justified by the flow dynamics at low magnetic Reynolds numbers. In this regime, the fluid velocity is small and imposed magnetic field dominates over fluid-induced perturbations, rendering the induced field negligible. Consequently, this permits a reduction (the low- Rm or inductionless approximation) of the full pre-Maxwell equations to a quasi-static formulation analogous to Darcy’s law, where only current density and electric potential require computation; see Remark 1 or [12] for a physical justification. Building upon this reduced modeling, the resulting MHD system, i.e., the inductionless MHD equations, significantly benefits mathematical analysis and facilitates numerical design.

As mentioned previously, our framework exploits phase-field methods to characterize dynamic interfaces in computations. Contrary to the aforementioned approaches, this methodology regards the interface as a thin transition layer where fluid properties can change smoothly. Correspondingly, it requires solving a fourth-order nonlinear partial differential equation (the Cahn–Hilliard equation) rather than linear equations typical of established methods. However, this can be efficiently addressed by mixed finite element methods [13] and linearizing techniques [50]. Additionally, phase-field models inherently incorporate a thermodynamic framework and (energy) stability properties, whereas only geometric interface information is primarily provided in VOF and LS formulations. While numerous thermodynamically consistent phase-field methods have been developed for two-phase flows in the literature, they basically fall into two categories, i.e., mass-averaged velocity based models [3, 37, 51, 52, 54] and volume-averaged velocity based models [2, 54]. In the former formulations, the mass conservation equation replaces the incompressibility constraint, resulting in a quasi-incompressible system. In contrast, the latter ones preserve the incompressibility condition, in turn maintaining a globally solenoidal velocity field. However, it is noteworthy that in a recent work [54], ten Eikelder and collaborators have rigorously demonstrated that these classes of models are fundamentally equivalent within the continuum mixture theory, except for the so-called Abels–Garcke–Grün (AGG) model [2], whose assumptions deviate from the underlying theoretical framework of [54]. Although a unified physical framework has been established by ten Eikelder et al. [54], we still adopts the ansatz of AGG model, justified by: (i) substantial investigations on two-phase flows using AGG model, evidenced by numerous well-designed algorithms [9, 17, 22, 35, 50, 57, 61, 63] and diverse multi-physics generalizations [8, 18, 25, 47, 60]; and (ii) rigorous mathematical theory on AGG model, ranging from asymptotic results [2] to global regularity [1].

With these techniques, we first formulate an underlying sharp-interface model, characterized by the fact that evolving interfaces are codimension-1 manifolds from a macroscopic perspective. The properties (mass conservation and energy identity) of this system are detailed in Theorem 1. Subsequently, to characterize the interface, we employ phase-field methods on this novel formulation and derive a model in terms of the volume-averaged velocity [2] according to Onsager’s variational principle [46]. By construction, this model admits thermodynamic consistency and conserves global mass, while holding an energy law that is not an obvious approximation of the sharp-interface counterpart; see Theorem 2.

To validate the phase-field method theoretically, we investigate the sharp-interface limit via method of matched asymptotic expansions, which is available for such a coupled system. This argument depends on two critical assumptions: (i) with vanishing interface thickness the domain can be decomposed into two distinct subdomains separated by an interface, each containing only one fluid; and (ii) the solutions admit separate asymptotic expansions in terms of interface thickness in the bulk and near the interface, which must be matched in the overlapping region. Following the techniques presented in [2, 59], we are able to deduce the convergence of our phase-field model to the intrinsic sharp-interface system under a parameter scaling law proposed by Magaletti et al. [39]. At a theoretical level, this result confirms the validity of our phase-field method as an approximated approach to model two-phase MHD flows.

In order to numerically verify the capability of our framework, we carry out a three-dimensional numerical example to explore the magnetic damping effects on bubble dynamics. To conduct such simulations, we develop a numerical algorithm based on a dimensionless form of the phase-field model. This algorithm utilizes backward difference formula of order k (BDF- k) and finite element method for temporal and spatial discretizations. And it incorporates a linearizing technique in [50] and the pressure stabilization method [26] to achieve a decoupled and linear structure, yielding straightforward implementations. Using this algorithm, we generalize a classical two-phase flow benchmark of Hysing et al. [31] to incorporate MHD effects. And

the observed phenomena are consistent with the results from Ni and collaborators [64, 65, 67], illustrating the effectiveness of our framework to accurately capture intricate MHD effects in two-phase flows.

The remainder of this paper is organized as follows. In Section 2 we establish the theoretical framework of two-phase MHD flows. Section 3 discusses the details of sharp-interface asymptotics. We present our numerical scheme and simulation results in Section 4. Finally, some conclusions and future research directions are given in Section 5.

2. Governing equations

2.1. Sharp-interface formulation

Consider a bounded domain $\Omega = \Omega_+(t) \cup \Omega_-(t) \subset \mathbb{R}^3$ containing two immiscible and incompressible fluids. Let \mathbf{u} , p , \mathbf{J} , V denote the fluid velocity, pressure, current density, and electric potential, respectively. For a magnetic Reynolds number $\text{Rm} \ll 1$, the flow dynamics subject to a steady external magnetic field \mathbf{B} in Ω_\pm are governed by the inductionless MHD equations (see Remark 1 for a physical justification of equations (1c)-(1d)),

$$\rho_\pm (\partial_t \mathbf{u} + \mathbf{u} \cdot \nabla \mathbf{u}) = \nabla \cdot (2\eta_\pm \mathbf{D}(\mathbf{u}) - p\mathbf{I}) + \mathbf{J} \times \mathbf{B} + \rho_\pm \mathbf{g}, \quad (1a)$$

$$\nabla \cdot \mathbf{u} = 0, \quad (1b)$$

$$\mathbf{J} = \sigma_\pm (-\nabla V + \mathbf{u} \times \mathbf{B}), \quad (1c)$$

$$\nabla \cdot \mathbf{J} = 0, \quad (1d)$$

where $\mathbf{D}(\mathbf{u}) = \frac{1}{2} (\nabla \mathbf{u} + (\nabla \mathbf{u})^\top)$ and \mathbf{I} are the deformation tensor and identity tensor. In this system, ρ_\pm , η_\pm and σ_\pm are the densities, dynamic viscosities and electrical conductivities of the two fluids, respectively. $\mathbf{g} = (0, 0, -g)^\top$ represents the gravitational acceleration with a positive constant g . Denote by $\Gamma(t) = \partial\Omega_+ \cap \partial\Omega_-$ the evolving interface between the two fluids, we define on Γ

$$[[2\eta \mathbf{D}(\mathbf{u}) - p\mathbf{I}]] \mathbf{n}_\Gamma = -\lambda \kappa \mathbf{n}_\Gamma, \quad (2a)$$

$$[[\mathbf{u}]] = 0, \quad (2b)$$

$$V_\Gamma = \mathbf{u} \cdot \mathbf{n}_\Gamma, \quad (2c)$$

$$[[\mathbf{J} \cdot \mathbf{n}_\Gamma]] = 0, \quad (2d)$$

$$[[V]] = 0, \quad (2e)$$

where we use the notation $\eta = \eta_+ \mathcal{X}_{\Omega_+} + \eta_- \mathcal{X}_{\Omega_-}$ (the same definition holds for ρ and σ) with \mathcal{X}_{Ω_\pm} being the characteristic function corresponding to Ω_\pm . λ , κ , \mathbf{n}_Γ and V_Γ stand for the surface tension, mean curvature, unit normal on Γ pointing to Ω_+ , and normal velocity of Γ . Generally, $[[\chi]]$ denotes the jump of quantity χ across Γ from Ω_+ to Ω_- . Equations (2a)-(2c) are standard jump conditions arising from two-phase incompressible flows [24], and equations (2d)-(2e) emerge naturally from electromagnetic theory.

To complete the system, some appropriate initial and boundary conditions need to be imposed. The initial data is set as

$$\mathbf{u}(0) = \mathbf{u}^0.$$

We only consider enclosed flows in this context. Hence, no-slip walls are imposed for \mathbf{u} , yielding

$$\mathbf{u} = \mathbf{0} \quad \text{on } \partial\Omega.$$

And insulating walls are applied for \mathbf{J} and V , which gives

$$\mathbf{J} \cdot \mathbf{n} = 0 \quad \text{on } \partial\Omega,$$

where \mathbf{n} is the unit outward normal to Ω . In some specific cases, such as aluminum reduction cells, conducting walls are required, resulting in mixed Dirichlet–Neumann boundary conditions,

$$\begin{aligned} \mathbf{J} \cdot \mathbf{n} &= \mathbf{J}_0 \cdot \mathbf{n} & \text{on } \partial\Omega_N, \\ V &= 0 & \text{on } \partial\Omega_D, \end{aligned}$$

where \mathbf{J}_0 is the applied current density and $\partial\Omega = \partial\Omega_N \cup \partial\Omega_D$. However, since \mathbf{J} and V obey a generalized Darcy’s law, it poses some challenges in energy and well-posedness analysis when involving conducting walls [14]. For simplicity, we only consider insulating walls in the following context.

Although a standard weak formulation for system (1)-(2) can be formulated [24], the phase-field methodology we utilized in this study differs from LS, VOF and FT approaches. It cannot be applied directly to sharp-interface formulations and must be derived from a thermodynamic framework. Therefore, we only give the properties of system (1)-(2) in the following theorem.

Theorem 1. *For system (1)-(2), there holds the individual mass conservation and energy dissipation law*

$$\begin{aligned} \frac{d}{dt} \int_{\Omega_{\pm}} \rho_{\pm} d\mathbf{x} &= 0, \\ \frac{d}{dt} \left(\int_{\Omega} \frac{1}{2} \rho |\mathbf{u}|^2 d\mathbf{x} + \int_{\Gamma} \lambda ds + \int_{\Omega} \rho g z d\mathbf{x} \right) &= - \int_{\Omega} 2\eta |\mathbf{D}(\mathbf{u})|^2 d\mathbf{x} - \int_{\Omega} \sigma^{-1} |\mathbf{J}|^2 d\mathbf{x} \leq 0, \end{aligned}$$

with $\mathbf{x} = (x, y, z)^{\top}$.

Proof. Exploiting the Reynolds transport theorem, we find [6]

$$\begin{aligned} \frac{d}{dt} \int_{\Omega_{\pm}} \rho_{\pm} d\mathbf{x} &= \int_{\Omega_{\pm}} \rho_{\pm} \nabla \cdot \mathbf{u} d\mathbf{x}, \\ \frac{d}{dt} \int_{\Omega_{\pm}} \frac{1}{2} \rho_{\pm} |\mathbf{u}|^2 d\mathbf{x} &= \int_{\Omega_{\pm}(t)} \rho_{\pm} (\partial_t \mathbf{u} + \mathbf{u} \cdot \nabla \mathbf{u}) \cdot \mathbf{u} d\mathbf{x}, \\ \frac{d}{dt} \int_{\Omega_{\pm}} \rho_{\pm} g z d\mathbf{x} &= - \int_{\Omega_{\pm}} \rho_{\pm} \mathbf{g} \cdot \mathbf{u} d\mathbf{x}, \\ \frac{d}{dt} \int_{\Gamma} \lambda ds &= - \int_{\Gamma} \lambda \kappa \mathbf{n}_{\Gamma} \cdot \mathbf{u} ds, \end{aligned}$$

which leads to

$$\begin{aligned} \frac{d}{dt} \int_{\Omega} \frac{1}{2} \rho |\mathbf{u}|^2 d\mathbf{x} &= \int_{\Omega} (\nabla \cdot (2\eta \mathbf{D}(\mathbf{u}) - p\mathbf{I}) + \mathbf{J} \times \mathbf{B} + \rho \mathbf{g}) \cdot \mathbf{u} d\mathbf{x} \\ &= - \int_{\Gamma} [2\eta \mathbf{D}(\mathbf{u}) - p\mathbf{I}] \mathbf{n}_{\Gamma} \cdot \mathbf{u} ds + \int_{\Omega} (-2\eta |\mathbf{D}(\mathbf{u})|^2 + \mathbf{J} \times \mathbf{B} \cdot \mathbf{u} + \rho \mathbf{g} \cdot \mathbf{u}) d\mathbf{x}. \end{aligned}$$

The proof is complete by invoking equations (1c)-(1d) and equations (2d)-(2e). \square

Remark 1. *Here we provide a physical justification of equations (1c)-(1d). The full pre-Maxwell equations read (we abuse the notations \mathbf{B} and σ to represent the magnetic field and electrical conductivity)*

$$\nabla \times \mathbf{B} = \mu_0 \mathbf{J}, \quad (3a)$$

$$\partial_t \mathbf{B} + \nabla \times \mathbf{E} = 0, \quad (3b)$$

$$\nabla \cdot \mathbf{B} = 0, \quad (3c)$$

$$\mathbf{J} = \sigma (\mathbf{E} + \mathbf{u} \times \mathbf{B}), \quad (3d)$$

where μ_0 and \mathbf{E} are the permeability of free space and electric field. Following [12], we use dimensional analysis to simplify the above equations. First, an external magnetic field \mathbf{B}_0 acts on the fluid, inducing a current density

$$\mathbf{J}_1 = \sigma \mathbf{u} \times \mathbf{B}_0.$$

Correspondingly, it gives rise to an induced magnetic field \mathbf{B}_1 , giving by Ampère's law,

$$\nabla \times \mathbf{B}_1 = \mu_0 \mathbf{J}_1.$$

This indicates that $|\mathbf{B}_1| \sim L_r \mu_0 \mathbf{J}_1 \sim \text{Rm} |\mathbf{B}_0|$, where $\text{Rm} = \mu_0 \sigma u_r L_r$ with u_r and L_r being the characteristic quantities of velocity and length. Hence, \mathbf{B}_1 is negligible by comparison with \mathbf{B}_0 when $\text{Rm} \ll 1$. Now consider the induced electric field \mathbf{E}_1 , Faraday's law and Ohm's law together yield (neglecting second-order term $\mathbf{u} \times \mathbf{B}_1$)

$$\begin{aligned} \nabla \times \mathbf{E}_1 &= -\partial_t \mathbf{B}_1, \\ \nabla \cdot \mathbf{E}_1 &= \nabla \cdot (\mathbf{u} \times \mathbf{B}_0). \end{aligned}$$

Applying the Helmholtz theorem, we can establish that to leading order in Rm , \mathbf{E}_1 is irrotational. Consequently, the total electric field admits the representation $\mathbf{E} = -\nabla V$ through an electric potential V . This yields a reduced Ohm's law,

$$\mathbf{J} = \sigma (-\nabla V + \mathbf{u} \times \mathbf{B}_0),$$

and the leading-order term in Lorentz force evidently becomes $\mathbf{J} \times \mathbf{B}_0$. Hence, in a low Rm regime, \mathbf{J} can be uniquely determined by

$$\mathbf{J} = \sigma (-\nabla V + \mathbf{u} \times \mathbf{B}_0), \quad (4a)$$

$$\nabla \cdot \mathbf{J} = 0, \quad (4b)$$

where the second equation is the charge conservation constraint that is implicitly contained within pre-Maxwell dynamics (readily verified by taking the divergence of Ampère's law).

2.2. Phase-field model

To employ the phase-field methodology, we assume a partial mixing of the two fluids in a narrow interfacial zone of thickness ϵ with volume incompressibility. For simplicity, we henceforth abuse the notations, such as ρ , η , etc. Let $V(t) \subset \Omega$ be an arbitrary control volume with its mass and density given by M and ρ . Then denote by M_{\pm} and ϱ_{\pm} the masses and densities of the two fluids in V , it holds that

$$\varrho_{\pm} = \frac{M_{\pm}}{V}, \rho = \frac{M}{V} = \frac{M_+ + M_-}{V} = \varrho_+ + \varrho_-.$$

In turn, the volume incompressibility assumption results in

$$1 = \frac{\frac{M_+}{\rho_+} + \frac{M_-}{\rho_-}}{V} = \frac{\varrho_+}{\rho_+} + \frac{\varrho_-}{\rho_-}.$$

Following [2], the order parameter for the mixture can be defined as

$$\phi = \frac{\varrho_+}{\rho_+} - \frac{\varrho_-}{\rho_-}, \quad (5)$$

which indicates that

$$\rho = \frac{\rho_+ - \rho_-}{2} \phi + \frac{\rho_+ + \rho_-}{2}. \quad (6)$$

Suppose these fluids move with different velocities \mathbf{u}_{\pm} , the continuity equations in the bulk read

$$\partial_t \varrho_{\pm} + \nabla \cdot (\varrho_{\pm} \mathbf{u}_{\pm}) = 0.$$

Then we can introduce the volume-averaged velocity and relative mass flux as

$$\mathbf{u} = \frac{\varrho_+}{\rho_+} \mathbf{u}_+ + \frac{\varrho_-}{\rho_-} \mathbf{u}_-,$$

$$\mathbf{J}_{\pm} = \varrho_{\pm} (\mathbf{u}_{\pm} - \mathbf{u}).$$

As a consequence,

$$\nabla \cdot \mathbf{u} = \nabla \cdot \left(\frac{\varrho_+}{\rho_+} \mathbf{u}_+ + \frac{\varrho_-}{\rho_-} \mathbf{u}_- \right) = -\partial_t \left(\frac{\varrho_+}{\rho_+} + \frac{\varrho_-}{\rho_-} \right) = 0,$$

and

$$\partial_t \phi = -\nabla \cdot \left(\frac{\varrho_+}{\rho_+} \mathbf{u} + \frac{\mathbf{J}_+}{\rho_+} - \frac{\varrho_-}{\rho_-} \mathbf{u} - \frac{\mathbf{J}_-}{\rho_-} \right) = -\nabla \cdot (\phi \mathbf{u} + \mathbf{J}_{\phi}),$$

where $\mathbf{J}_{\phi} = \frac{\mathbf{J}_+}{\rho_+} - \frac{\mathbf{J}_-}{\rho_-}$. Correspondingly, this implies that mass diffusion is permitted in our framework.

Hence, the momentum $\rho \mathbf{u}$ should be transported by $\rho \mathbf{u} + \frac{\partial \rho}{\partial \phi} \mathbf{J}_{\phi}$, giving

$$\rho \partial_t \mathbf{u} + \left(\rho \mathbf{u} + \frac{\partial \rho}{\partial \phi} \mathbf{J}_{\phi} \right) \cdot \nabla \mathbf{u} = \nabla \cdot \mathbf{S} - \nabla p + \mathbf{F},$$

where \mathbf{S} is a symmetric second-order tensor, p is the pressure serving as a Lagrange multiplier for the incompressibility constraint, and \mathbf{F} is a force density.

Invoking Ohm's law with charge conservation (4), we conclude

$$\partial_t \phi + \nabla \cdot (\phi \mathbf{u} + \mathbf{J}_\phi) = 0, \quad (7a)$$

$$\rho \partial_t \mathbf{u} + \left(\rho \mathbf{u} + \frac{\partial \rho}{\partial \phi} \mathbf{J}_\phi \right) \cdot \nabla \mathbf{u} = \nabla \cdot \mathbf{S} - \nabla p + \mathbf{F}, \quad (7b)$$

$$\nabla \cdot \mathbf{u} = 0, \quad (7c)$$

$$\mathbf{J} = \sigma(\phi) (-\nabla V + \mathbf{u} \times \mathbf{B}), \quad (7d)$$

$$\nabla \cdot \mathbf{J} = 0, \quad (7e)$$

with \mathbf{J}_ϕ , \mathbf{S} , and \mathbf{F} to be specified (the definition of σ will be given later). Notice that mass conservation requires

$$\mathbf{J}_\phi \cdot \mathbf{n} = 0 \quad \text{on } \partial\Omega.$$

To derive a thermodynamically consistent model, we employ Onsager's variational principle as in [2]. By introducing the Rayleighian functional

$$\mathcal{R} = \frac{d\mathcal{E}}{dt} + \mathcal{P}, \quad (8)$$

where \mathcal{E} and \mathcal{P} are the free energy and dissipation functional, Onsager's variational principle states that the kinetic equation is equivalent to the minimum of \mathcal{R} [46]. Then we define

$$\mathcal{E} = \int_{\Omega} \left(\frac{1}{2} \rho |\mathbf{u}|^2 + f(\phi, \nabla \phi) \right) d\mathbf{x}, \quad (9)$$

where $f(\phi, \nabla \phi)$ is a Helmholtz free energy density. Thus, it holds that

$$\begin{aligned} \frac{d\mathcal{E}}{dt} &= \int_{\Omega} \left(\frac{1}{2} \partial_t \rho |\mathbf{u}|^2 + \rho \mathbf{u} \cdot \partial_t \mathbf{u} + \mu \partial_t \phi \right) d\mathbf{x} \\ &= \int_{\Omega} (\mathbf{u} \cdot \nabla \cdot \mathbf{S} + \mathbf{u} \cdot \mathbf{F} - \mu \nabla \cdot (\phi \mathbf{u} + \mathbf{J}_\phi)) d\mathbf{x} \\ &= \int_{\Omega} (-\mathbf{S} : \mathbf{D}(\mathbf{u}) + \mathbf{u} \cdot \mathbf{F} - \mu \mathbf{u} \cdot \nabla \phi + \mathbf{J}_\phi \cdot \nabla \mu) d\mathbf{x}, \end{aligned}$$

where

$$\mu = \frac{\partial f}{\partial \phi} - \nabla \cdot \frac{\partial f}{\partial \nabla \phi}$$

is abbreviated to denote the chemical potential and we assume a vanishing normal component of $\frac{\partial f}{\partial \nabla \phi}$ on $\partial\Omega$. Since the first law of thermodynamics reads

$$\frac{d\mathcal{E}}{dt} = -\mathcal{T} \frac{d\mathcal{S}}{dt} + \frac{d\mathcal{W}}{dt}, \quad (10)$$

where \mathcal{T} , \mathcal{S} , and \mathcal{W} represent the temperature, entropy, and mechanical work, we are able to identify

$$\frac{d\mathcal{W}}{dt} = \int_{\Omega} (\mathbf{u} \cdot \mathbf{F} - \mu \mathbf{u} \cdot \nabla \phi) d\mathbf{x}.$$

Incorporating external gravitational and Lorentz forces, \mathbf{F} is given by

$$\mathbf{F} = \mu \nabla \phi + \mathbf{J} \times \mathbf{B} + \rho \mathbf{g}.$$

To further specify \mathbf{S} and \mathbf{J}_ϕ , we introduce the dissipation functional

$$\mathcal{P} = \int_{\Omega} \left(\frac{|\mathbf{S}|^2}{4\eta(\phi)} + \frac{|\mathbf{J}_\phi|^2}{2M(\phi)} + \frac{|\mathbf{J}|^2}{2\sigma(\phi)} \right) d\mathbf{x}, \quad (11)$$

which accounts for viscous dissipation, diffusive dissipation, and Ohmic dissipation, respectively, and M is the mobility which plays the role of diffusivity for diffuse interfaces. In accordance to Onsager's variational principle, we get

$$\mathbf{S} = 2\eta \mathbf{D}(\mathbf{u}) \quad \text{and} \quad \mathbf{J}_\phi = -M(\phi) \nabla \mu.$$

In this work, we consider the Helmholtz free energy density in the Ginzburg-Landau form:

$$f(\phi, \nabla\phi) = \frac{\hat{\lambda}\epsilon}{2} |\nabla\phi|^2 + \frac{\hat{\lambda}\epsilon^{-1}}{4} (\phi^2 - 1)^2, \quad (12)$$

where $\hat{\lambda} = \frac{3\lambda}{2\sqrt{2}}$ is the scaled surface tension, and we obtain

$$\partial_t\phi + \nabla \cdot (\phi\mathbf{u}) = \nabla \cdot (M\nabla\mu), \quad (13a)$$

$$\mu = -\hat{\lambda}\epsilon\Delta\phi + \hat{\lambda}\epsilon^{-1}(\phi^3 - \phi), \quad (13b)$$

$$\rho\partial_t\mathbf{u} + \left(\rho\mathbf{u} - \frac{\partial\rho}{\partial\phi}M\nabla\mu\right) \cdot \nabla\mathbf{u} = \nabla \cdot (2\eta\mathbf{D}(\mathbf{u}) - p\mathbf{I}) + \mu\nabla\phi + \mathbf{J} \times \mathbf{B} + \rho\mathbf{g}, \quad (13c)$$

$$\nabla \cdot \mathbf{u} = 0, \quad (13d)$$

$$\mathbf{J} = \sigma(-\nabla V + \mathbf{u} \times \mathbf{B}), \quad (13e)$$

$$\nabla \cdot \mathbf{J} = 0. \quad (13f)$$

Here we assume that η and σ linearly depend on ϕ ,

$$\eta = \frac{\eta_+ - \eta_-}{2}\phi + \frac{\eta_+ + \eta_-}{2} \quad \text{and} \quad \sigma = \frac{\sigma_+ - \sigma_-}{2}\phi + \frac{\sigma_+ + \sigma_-}{2},$$

so that the model is compatible with the inductionless MHD equations in the single fluid regime. Mass conservation gives no-flux walls for ϕ and μ :

$$\nabla\phi \cdot \mathbf{n} = 0 \quad \text{on} \quad \partial\Omega,$$

$$\nabla\mu \cdot \mathbf{n} = 0 \quad \text{on} \quad \partial\Omega.$$

Together with initial condition

$$\phi(0) = \phi^0,$$

the system is closed.

In the case of sharp-interface system described by equations (1)-(2), individual mass is preserved. However, for the derived phase-field model given by equations (13), only global mass conservation can be ensured. Moreover, the energy of this model no longer exhibits a dissipative feature.

Theorem 2. *For system (13), there holds the global mass conservation and energy law*

$$\begin{aligned} \frac{d}{dt} \int_{\Omega} \phi d\mathbf{x} &= 0, \\ \frac{d}{dt} \left(\int_{\Omega} \frac{1}{2} \rho |\mathbf{u}|^2 d\mathbf{x} + \int_{\Omega} f(\phi, \nabla\phi) d\mathbf{x} \right) &= - \int_{\Omega} M |\nabla\mu|^2 d\mathbf{x} - \int_{\Omega} 2\eta |\mathbf{D}(\mathbf{u})|^2 d\mathbf{x} - \int_{\Omega} \sigma^{-1} |\mathbf{J}|^2 d\mathbf{x} + \int_{\Omega} \rho \mathbf{g} \cdot \mathbf{u} d\mathbf{x}. \end{aligned}$$

Proof. As the proof follows routine procedures, details are not presented. \square

In phase-field simulations, an appropriate choice of parameters ϵ and M is essential to make computations both affordable and comparable with analytical or experimental results. Here we take a constant M with a scaling law $M = \mathcal{O}(\epsilon^2)$ suggested by Magaletti et al. [39], which has been utilized widely [35, 57, 60]. This scaling law facilitates the asymptotic analysis by rendering the extra flux term $M\nabla\mu$ in the momentum equation a higher-order contribution with respect to interface thickness. Consequently, this term does not affect the leading-order dynamics, ensuring that the correct physical behavior is preserved in the sharp-interface asymptotics; see [2] for several scalings that may lead to a nonstandard sharp-interface model.

3. Sharp-interface asymptotics

3.1. Preliminaries

For a solution $(\phi_\epsilon, \mu_\epsilon, \mathbf{u}_\epsilon, p_\epsilon, \mathbf{J}_\epsilon, V_\epsilon)$ of system (13), we assume that it converges formally to a limit $(\phi, \mu, \mathbf{u}, p, \mathbf{J}, V)$ as interface thickness $\epsilon \rightarrow 0$. And we further assume

$$\Omega_+ = \{\mathbf{x} \in \Omega : \phi_\epsilon(\mathbf{x}) > 0\} \quad \text{and} \quad \Omega_- = \{\mathbf{x} \in \Omega : \phi_\epsilon(\mathbf{x}) < 0\}.$$

The corresponding interface that separates Ω_{\pm} is denoted by

$$\Gamma = \{\mathbf{x} \in \Omega : \phi_{\epsilon}(\mathbf{x}) = 0\}.$$

In outer regions far from Γ , there holds the outer expansions with respect to interface thickness ϵ of ϕ_{ϵ} , \mathbf{u}_{ϵ} , p_{ϵ} , \mathbf{J}_{ϵ} , V_{ϵ} in the form (exemplarily for ϕ_{ϵ})

$$\phi_{\epsilon} = \phi_0^{\pm} + \epsilon\phi_1^{\pm} + \epsilon^2\phi_2^{\pm} + \dots.$$

As an auxiliary variable, we have evidently for μ :

$$\mu_{\epsilon} = \epsilon^{-1}\mu_0^{\pm} + \mu_1^{\pm} + \epsilon\mu_2^{\pm} + \dots$$

where $\mu_0^{\pm} = \widehat{\lambda}((\phi_0^{\pm})^3 - \phi_0^{\pm})$. In the transition layer near Γ , we introduce a new stretched coordinates to scale the variables. Let $d(\mathbf{x})$ be the signed distance function to Γ such that $d(\mathbf{x}) > 0$ if $\mathbf{x} \in \Omega_{+}$, then we have $\mathbf{n}_{\Gamma} = \nabla d$ and $V_{\Gamma} = -\partial_t d$. Defining the scaled distance $z = \frac{d}{\epsilon}$, the following change of variables holds [2, 47]:

$$\partial_t \chi = -\epsilon^{-1} V_{\Gamma} \partial_z \chi + \mathcal{O}(1), \quad (14a)$$

$$\nabla \chi = \epsilon^{-1} \partial_z \chi \mathbf{n}_{\Gamma} + \nabla_{\Gamma} \chi + \mathcal{O}(\epsilon), \quad (14b)$$

$$\nabla \cdot \chi = \epsilon^{-1} \partial_z \chi \cdot \mathbf{n}_{\Gamma} + \nabla_{\Gamma} \cdot \chi + \mathcal{O}(\epsilon), \quad (14c)$$

$$\nabla \chi = \epsilon^{-1} \partial_z \chi \otimes \mathbf{n}_{\Gamma} + \nabla_{\Gamma} \chi + \mathcal{O}(\epsilon), \quad (14d)$$

$$\Delta \chi = \epsilon^{-2} \partial_{zz} \chi - \epsilon^{-1} \kappa \partial_z \chi + \mathcal{O}(1), \quad (14e)$$

where χ and χ are generic scalar-valued and vector-valued variables. Then in this region we have inner expansions in terms of interface thickness ϵ for ϕ_{ϵ} , \mathbf{u}_{ϵ} , p_{ϵ} , \mathbf{J}_{ϵ} , V_{ϵ} in the form (also exemplarily for ϕ_{ϵ})

$$\phi_{\epsilon} = \phi_0^i + \epsilon\phi_1^i + \epsilon^2\phi_2^i + \dots,$$

with $\mu_{\epsilon} = \epsilon^{-1}\mu_0^i + \mu_1^i + \epsilon\mu_2^i + \dots$, where

$$\mu_0^i = \widehat{\lambda}(-\partial_{zz}\phi_0^i + (\phi_0^i)^3 - \phi_0^i),$$

$$\mu_1^i = \widehat{\lambda}(-\partial_{zz}\phi_1^i + \kappa\partial_z\phi_0^i + (3(\phi_0^i)^2 - 1)\phi_1^i).$$

In an overlapping region, outer and inner expansions must satisfy the matching conditions [2, 47]

$$\lim_{z \rightarrow \pm\infty} \chi_0^i = \chi_0^{\pm}, \quad (15a)$$

$$\lim_{z \rightarrow \pm\infty} \partial_z \chi_0^i = 0, \quad (15b)$$

$$\lim_{z \rightarrow \pm\infty} \partial_z \chi_1^i = \nabla \chi_0^{\pm} \cdot \mathbf{n}_{\Gamma}, \quad (15c)$$

where χ is a generic variable.

Following the procedure in [2, 59], we will establish that the limit solution $(\phi, \mu, \mathbf{u}, p, \mathbf{J}, V)$ exactly satisfies the sharp-interface system (1)-(2).

3.2. Bulk equations

Expansion of (13c) at order $\mathcal{O}(\epsilon^{-1})$: Recalling $M = \mathcal{O}(\epsilon^2)$, where we assume $M = m\epsilon^2$ in the following context, the leading order of the flux $M\nabla\mu$ is $\mathcal{O}(\epsilon)$. Hence, we obtain

$$\mu_0^{\pm} \nabla \phi_0^{\pm} = 0,$$

which is equivalent to

$$\nabla \frac{((\phi_0^{\pm})^2 - 1)^2}{4} = 0. \quad (16)$$

This implies that $\phi_0^{\pm} = c_{\pm}$ with c_{\pm} two constants such that $c_{+} > 0$ and $c_{-} < 0$.

Expansion of (13c)-(13f) at order $\mathcal{O}(1)$: Using the fact that $M\nabla\mu$ is of order $\mathcal{O}(\epsilon)$, we conclude

$$\rho_0^{\pm} (\partial_t \mathbf{u}_0^{\pm} + \mathbf{u}_0^{\pm} \cdot \nabla \mathbf{u}_0^{\pm}) = \nabla \cdot (2\eta_0^{\pm} \mathbf{D}(\mathbf{u}_0^{\pm})) - \nabla p_0^{\pm} + \mu_0^{\pm} \nabla \phi_1^{\pm} + \mathbf{J}_0^{\pm} \times \mathbf{B} + \rho_0^{\pm} \mathbf{g}, \quad (17a)$$

$$\nabla \cdot \mathbf{u}_0^{\pm} = 0, \quad (17b)$$

$$\mathbf{J}_0^{\pm} = \sigma_0^{\pm} (-\nabla V_0^{\pm} + \mathbf{u}_0^{\pm} \times \mathbf{B}), \quad (17c)$$

$$\nabla \cdot \mathbf{J}_0^{\pm} = 0, \quad (17d)$$

where we abbreviate $\chi_0^{\pm} = \frac{\chi_{+} - \chi_{-}}{2} \phi_0^{\pm} + \frac{\chi_{+} + \chi_{-}}{2}$ for ρ , η , and σ .

3.3. Jump conditions

Expansion of (13d) at order $\mathcal{O}(\epsilon^{-1})$: Invoking change of variables (14), we get

$$\partial_z \mathbf{u}_0^i \cdot \mathbf{n}_\Gamma = 0, \quad (18)$$

which implies that $\mathbf{u}_0^i \cdot \mathbf{n}_\Gamma$ does not depend on z .

Expansion of (13a) at order $\mathcal{O}(\epsilon^{-1})$: With a similar procedure, we obtain

$$-V_\Gamma \partial_z \phi_0^i + \partial_z (\phi_0^i \mathbf{u}_0^i) \cdot \mathbf{n}_\Gamma = m \partial_{zz} \mu_0^i.$$

Integrating this equation with respect to z from $-\infty$ to ∞ yields

$$(-V_\Gamma + \mathbf{u}_0^i \cdot \mathbf{n}_\Gamma) \int_{-\infty}^{\infty} \partial_z \phi_0^i dz = m \int_{-\infty}^{\infty} \partial_{zz} \mu_0^i dz.$$

Then matching conditions (15a)-(15b) require

$$(-V_\Gamma + \mathbf{u}_0^i \cdot \mathbf{n}_\Gamma) (\phi_0^+ - \phi_0^-) = 0,$$

in turn giving

$$V_\Gamma = \mathbf{u}_0^i \cdot \mathbf{n}_\Gamma. \quad (19)$$

Additionally, we have

$$\partial_{zz} \mu_0^i = 0,$$

or equivalently, μ_0^i linearly depends on z . Required by matching condition (15a), we conclude that μ_0^i has to be a constant.

Expansion of (13c) at order $\mathcal{O}(\epsilon^{-2})$: Denoting by $\mathcal{D}(\mathbf{A}) = \frac{1}{2}(\mathbf{A} + \mathbf{A}^\top)$, we obtain after the change of variables (14),

$$\nabla \cdot (2\eta \mathbf{D}(\mathbf{u})) = \epsilon^{-2} \partial_z (2\eta \mathcal{D}(\partial_z \mathbf{u} \otimes \mathbf{n}_\Gamma) \mathbf{n}_\Gamma) + \epsilon^{-1} \partial_z (2\eta \mathcal{D}(\nabla_\Gamma \mathbf{u}) \mathbf{n}_\Gamma) + \epsilon^{-1} \nabla_\Gamma \cdot (2\eta \mathcal{D}(\partial_z \mathbf{u} \otimes \mathbf{n}_\Gamma) + \mathcal{O}(1)). \quad (20)$$

Notice that $M \nabla \mu$ is of order $\mathcal{O}(\epsilon)$ in inner region since μ_0^i is independent of z , we conclude

$$\partial_z (\eta_0^i \partial_z \mathbf{u}_0^i) + \mu_0^i \partial_z \phi_0^i \mathbf{n}_\Gamma = 0,$$

where we have used

$$(\mathbf{n}_\Gamma \otimes \partial_z \mathbf{u}_0^i) \mathbf{n}_\Gamma = (\partial_z \mathbf{u}_0^i \cdot \mathbf{n}_\Gamma) \mathbf{n}_\Gamma = 0.$$

We integrate this equation with respect to z and obtain

$$\eta_0^i \partial_z \mathbf{u}_0^i|_{-\infty}^{\infty} + \mu_0^i \phi_0^i|_{-\infty}^{\infty} \mathbf{n}_\Gamma = 0.$$

Through equation (18), taking an inner product with \mathbf{n}_Γ and matching condition (15a) yield

$$\mu_0^i (\phi_0^+ - \phi_0^-) = 0,$$

in turn indicating $\mu_0^i = 0$, or equivalently

$$-\partial_{zz} \phi_0^i + (\phi_0^i)^3 - \phi_0^i = 0. \quad (21)$$

The solvability of this equation [45, 59] leads to

$$\phi_0^\pm = \lim_{z \rightarrow \pm\infty} \phi_0^i = \pm 1 \quad \text{and} \quad \phi_0^i = \tanh \frac{z}{\sqrt{2}}. \quad (22)$$

Then we have a second-order ordinary differential equation

$$\partial_z (\eta_0^i \partial_z \mathbf{u}_0^i) = 0,$$

which by matching conditions (15a)-(15b) and positivity of η , implies that \mathbf{u}_0^i is independent of z [2]. Hence, we obtain

$$\llbracket \mathbf{u}_0^\pm \rrbracket = 0. \quad (23)$$

Expansion of (13c) at order $\mathcal{O}(\epsilon^{-1})$: Combining matching conditions (15a) and (15c) we have

$$\lim_{z \rightarrow \pm\infty} (\partial_z \mathbf{u}_1^i \otimes \mathbf{n}_\Gamma + \nabla_\Gamma \mathbf{u}_0^i) = \nabla \mathbf{u}_0^\pm. \quad (24)$$

Notice that \mathbf{u}_0^i and μ_0^i are indeed constants, we find

$$\partial_z (2\eta_0^i \mathcal{D}(\partial_z \mathbf{u}_1^i \otimes \mathbf{n}_\Gamma) \mathbf{n}_\Gamma) + \partial_z (2\eta_0^i \mathcal{D}(\nabla_\Gamma \mathbf{u}_0^i) \mathbf{n}_\Gamma) - \partial_z p_0^i \mathbf{n}_\Gamma + \mu_1^i \partial_z \phi_0^i \mathbf{n}_\Gamma = 0.$$

Then integrating and using matching conditions (15a) and (24) yield

$$\llbracket 2\eta_0^\pm \mathbf{D}(\mathbf{u}_0^\pm) - p_0^\pm \mathbf{I} \rrbracket \mathbf{n}_\Gamma = - \int_{-\infty}^{\infty} \mu_1^i \partial_z \phi_0^i \mathbf{n}_\Gamma dz.$$

For the right-hand side of this equation, integration by parts with matching conditions (15a)-(15b) leads to

$$\begin{aligned} \int_{-\infty}^{\infty} \mu_1^i \partial_z \phi_0^i dz &= \hat{\lambda} \int_{-\infty}^{\infty} (-\partial_{zz} \phi_1^i + \kappa \partial_z \phi_0^i + (3(\phi_0^i)^2 - 1)\phi_1^i) \partial_z \phi_0^i dz, \\ &= \hat{\lambda} \kappa \int_{-\infty}^{\infty} (\partial_z \phi_0^i)^2 dz + \hat{\lambda} \int_{-\infty}^{\infty} (-\partial_{zz} \phi_1^i + (3(\phi_0^i)^2 - 1)\phi_1^i) \partial_z \phi_0^i dz \\ &= \frac{2\sqrt{2}\hat{\lambda}\kappa}{3} + \hat{\lambda} \int_{-\infty}^{\infty} (\partial_{zz} \phi_0^i - (\phi_0^i)^3 + \phi_0^i) \partial_z \phi_1^i dz \\ &= \lambda \kappa, \end{aligned}$$

where

$$\int_{-\infty}^{\infty} (\partial_z \phi_0^i)^2 dz = \frac{1}{2} \int_{-\infty}^{\infty} \text{sech}^4 \frac{z}{\sqrt{2}} dz = \frac{2\sqrt{2}}{3}.$$

Then we conclude

$$\llbracket 2\eta_0^\pm \mathbf{D}(\mathbf{u}_0^\pm) - p_0^\pm \mathbf{I} \rrbracket \mathbf{n}_\Gamma = -\lambda \kappa. \quad (25)$$

Expansion of (13e)-(13f) at order $\mathcal{O}(\epsilon^{-1})$: A direct change of variables (14) gives

$$\begin{aligned} \partial_z \varphi_0^i \mathbf{n}_\Gamma &= \mathbf{0}, \\ \partial_z \mathbf{J}_0^i \cdot \mathbf{n}_\Gamma &= 0. \end{aligned}$$

With matching condition (15a), we obtain

$$\llbracket V_0^\pm \rrbracket = 0, \quad (26a)$$

$$\llbracket \mathbf{J}_0^\pm \cdot \mathbf{n}_\Gamma \rrbracket = 0. \quad (26b)$$

3.4. Summary of sharp-interface limit

Here we summarize the main results. First, in region far from Γ , we have $\phi_0^\pm = \pm 1$ and $\mu_0^\pm = 0$. Then the bulk equations read

$$\rho_\pm (\partial_t \mathbf{u}_0^\pm + \mathbf{u}_0^\pm \cdot \nabla \mathbf{u}_0^\pm) = \nabla \cdot (2\eta_0^\pm \mathbf{D}(\mathbf{u}_0^\pm) - p_0^\pm \mathbf{I}) + \mathbf{J}_0^\pm \times \mathbf{B} + \rho_0^\pm \mathbf{g}, \quad (27a)$$

$$\nabla \cdot \mathbf{u}_0^\pm = 0, \quad (27b)$$

$$\mathbf{J}_0^\pm = \sigma_\pm (-\nabla V_0^\pm + \mathbf{u}_0^\pm \times \mathbf{B}), \quad (27c)$$

$$\nabla \cdot \mathbf{J}_0^\pm = 0, \quad (27d)$$

and the jump conditions are

$$\llbracket 2\eta_0^\pm \mathbf{D}(\mathbf{u}_0^\pm) - p_0^\pm \mathbf{I} \rrbracket \mathbf{n}_\Gamma = -\lambda \kappa, \quad (28a)$$

$$\llbracket \mathbf{u}_0^\pm \rrbracket = 0, \quad (28b)$$

$$V_\Gamma = \mathbf{u}_0^i \cdot \mathbf{n}_\Gamma, \quad (28c)$$

$$\llbracket V_0^\pm \rrbracket = 0, \quad (28d)$$

$$\llbracket \mathbf{J}_0^\pm \cdot \mathbf{n}_\Gamma \rrbracket = 0. \quad (28e)$$

As $\epsilon \rightarrow 0$, we can deduce that the limit system is the aforementioned sharp-interface model (1)-(2). This illustrates the reliability of model (13) as an approximated approach with regard to system (1)-(2).

4. Numerical simulation

4.1. Non-dimensionalization and discrete scheme

Let ρ_r , η_r , σ_r and B_r denote the characteristic quantities of density, dynamic viscosity, electrical conductivity and magnetic field, respectively (recall that L_r and u_r are characteristic length and velocity). We introduce the following scalings:

$$\begin{aligned} \mathbf{x} &\leftarrow \frac{\mathbf{x}}{L_r}, \quad t \leftarrow \frac{tu_r}{L_r}, \quad \mathbf{u} \leftarrow \frac{\mathbf{u}}{u_r}, \quad \rho \leftarrow \frac{\rho}{\rho_r}, \quad \eta \leftarrow \frac{\eta}{\eta_r}, \quad p \leftarrow \frac{p}{\rho_r u_r^2}, \\ \mu &\leftarrow \frac{\mu\epsilon}{\widehat{\lambda}}, \quad V \leftarrow \frac{V}{L_r u_r B_r}, \quad \mathbf{J} \leftarrow \frac{\mathbf{J}}{\sigma_r u_r B_r}, \quad \sigma \leftarrow \frac{\sigma}{\sigma_r}. \end{aligned} \quad (29)$$

Of course, the dimensionless system is given by

$$\partial_t \phi + \nabla \cdot (\phi \mathbf{u}) = \frac{1}{\text{Pe}} \Delta \mu, \quad (30a)$$

$$\mu = -\text{Cn}^2 \Delta \phi + \phi^3 - \phi, \quad (30b)$$

$$\rho \partial_t \mathbf{u} + \left(\rho \mathbf{u} - \frac{\partial \rho}{\partial \phi} \frac{1}{\text{Pe}} \nabla \mu \right) \cdot \nabla \mathbf{u} = \frac{1}{\text{Re}} \nabla \cdot (2\eta \mathbf{D}(\mathbf{u})) - \nabla p + \frac{1}{\text{WeCn}} \mu \nabla \phi + \text{N} \mathbf{J} \times \mathbf{B} - \frac{1}{\text{Fr}} \rho \mathbf{e}_3, \quad (30c)$$

$$\nabla \cdot \mathbf{u} = 0, \quad (30d)$$

$$\mathbf{J} = \sigma (-\nabla V + \mathbf{u} \times \mathbf{B}), \quad (30e)$$

$$\nabla \cdot \mathbf{J} = 0, \quad (30f)$$

where $\mathbf{e}_3 = (0, 0, 1)^\top$. And the dimensionless numbers are

- Cahn number $\text{Cn} = \frac{\epsilon}{L_r}$ (interface thickness);
- Péclet number $\text{Pe} = \frac{\epsilon L_r u_r}{\widehat{\lambda} M}$ (ratio of interface thickness to mobility);
- Reynolds number $\text{Re} = \frac{L_r \rho_r u_r}{\eta_r}$ (ratio of the inertial to viscous forces);
- Weber number $\text{We} = \frac{L_r \rho_r u_r^2}{\widehat{\lambda}}$ (ratio of inertial to interfacial forces);
- Stuart number $\text{N} = \frac{L_r \sigma_r B^2}{\rho_r u_r}$ (ratio of electromagnetic to inertial forces);
- Froude number $\text{Fr} = \frac{u_r^2}{gL_r}$ (ratio of inertial to gravitational acceleration forces).

In this scaling, we apply the scaling law $\frac{1}{\text{Pe}} = 3\text{Cn}$ given by Magaletti et al. [39].

Let $V_h \subset H^1(\Omega)$, $\mathbf{X}_h \subset H_0^1(\Omega)^3$, $M_h \subset L_0^2(\Omega) \cap H^1(\Omega)$ be the Lagrange finite element spaces, and we use a uniform partition of the time interval $[0, T]$ with time step size τ , with the following BDF operator is defined:

$$\delta_\tau \chi^{n+1} = \frac{\gamma_0 \chi^{n+1} - \hat{\chi}}{\tau},$$

where χ is a generic variable, and

$$\hat{\chi} = \begin{cases} \chi^n, & k=1, \\ 2\chi^n - \frac{1}{2}\chi^{n-1}, & k=2, \end{cases}; \quad \gamma_0 = \begin{cases} 1, & k=1, \\ 3/2, & k=2. \end{cases}$$

We also recall the extrapolation formulas:

$$\widetilde{\chi}^{n+1} = \begin{cases} \chi^n, & k=1, \\ 2\chi^n - \chi^{n-1}, & k=2. \end{cases}$$

With these notations, the discrete BDF- k finite element scheme is given as follows:

Step 1: find $(\phi^{n+1}, \mu^{n+1}) \in V_h \times V_h$, such that for all $(\psi_h, \omega_h) \in V_h \times V_h$,

$$\begin{aligned} (\delta_\tau \phi_h^{n+1}, \omega_h) + \frac{1}{\text{Pe}} (\nabla \mu_h^{n+1}, \nabla \omega_h) &= (\tilde{\phi}_h^{n+1} \tilde{\mathbf{u}}_h^{n+1}, \nabla \omega_h), \\ (\mu_h^{n+1}, \psi_h) - \text{Cn}^2 (\nabla \phi_h^{n+1}, \nabla \psi_h) - (\phi_h^{n+1}, \psi_h) &= ((\tilde{\phi}_h^{n+1})^3 - 2\tilde{\phi}_h^{n+1}). \end{aligned} \quad (31)$$

Then we evaluate ρ_h^{n+1} , η_h^{n+1} and σ_h^{n+1} by (exemplarily for ρ_h^{n+1})

$$\rho_h^{n+1} = \frac{\rho_+ - \rho_-}{2\rho_r} \mathcal{C}(\phi_h^{n+1}) + \frac{\rho_+ + \rho_-}{2\rho_r},$$

where

$$\mathcal{C}(\phi_h^{n+1}) = \begin{cases} \phi_h^{n+1}, & \text{if } |\phi_h^{n+1}| \leq 1, \\ \text{sign}(\phi_h^{n+1}), & \text{otherwise.} \end{cases}$$

Step 2: find $\mathbf{u}_h^{n+1} \in \mathbf{X}_h$, such that for all $\mathbf{v}_h \in \mathbf{X}_h$,

$$\begin{aligned} (\rho_h^{n+1} \delta_\tau \mathbf{u}_h^{n+1}, \mathbf{v}_h) + \frac{2}{\text{Re}} (\eta_h^{n+1} \mathbf{D}(\mathbf{u}_h^{n+1}), \mathbf{D}(\mathbf{v}_h)) &= - \left(\left(\rho_h^{n+1} \tilde{\mathbf{u}}_h^{n+1} - \frac{\partial \rho}{\partial \phi} \frac{1}{\text{Pe}} \nabla \mu_h^{n+1} \right) \cdot \nabla \tilde{\mathbf{u}}_h^{n+1}, \mathbf{v}_h \right) \\ &\quad + (\tilde{p}_h^{n+1}, \nabla \cdot \mathbf{v}_h) + \frac{1}{\text{WeCn}} (\mu_h^{n+1} \nabla \phi_h^{n+1}, \mathbf{v}_h) \\ &\quad + (\tilde{\mathbf{J}}_h^{n+1} \times \mathbf{B}, \mathbf{v}_h) + (\rho_h^{n+1} \mathbf{e}_3, \mathbf{v}_h). \end{aligned} \quad (32)$$

Step 3: find $p_h^{n+1} \in M_h$, such that for all $q_h \in M_h$,

$$(\nabla(p_h^{n+1} - p_h^n), \nabla q_h) = -\frac{\gamma_0 \zeta}{\tau} (\nabla \cdot \mathbf{u}_h^{n+1}, q_h), \quad (33)$$

where $\zeta = \frac{\min(\rho_+, \rho_-)}{\rho_r}$.

Step 4: find $V_h^{n+1} \in M_h$, such that for all $\Lambda_h \in M_h$

$$(\sigma_h^{n+1} \nabla V_h^{n+1}, \nabla \Lambda_h) = (\sigma_h^{n+1} \mathbf{u}_h^{n+1} \times \mathbf{B}, \nabla \Lambda_h). \quad (34)$$

Then we evaluate $\mathbf{J}_h^{n+1} = \sigma_h^{n+1} (-\nabla V_h^{n+1} + \mathbf{u}_h^{n+1} \times \mathbf{B})$ when needed.

In the above scheme, we have exploited a linearizing technique in [50] and the pressure stabilization method developed by Guermond and Salgado [26]. Additionally, \mathbf{J} and V are solved in a primal formulation [14], due to the fact that σ will lead to a poorly scaled linear system in mixed formulation. While this scheme offers straightforward implementation, there exists two significant limitations: (i) absence of a discrete energy law, which is particularly desirable in phase-field computations [15, 68]; and (ii) non-conservative current density, which is important for accurate MHD simulations [36, 44]. Despite these restrictions, one can readily verify that the scheme (31)-(34) admits a unique solution and is globally mass conservative (we refer to [57] for some details),

$$\int_{\Omega} \phi_h^{n+1} d\mathbf{x} = \int_{\Omega} \phi_h^n d\mathbf{x}.$$

Remark 2. By its very definition, the order parameter ϕ should physically belong to $[-1, 1]$, yet the Ginzburg-Landau energy cannot guarantee this bound at a theoretical level, unlike the Flory-Huggins logarithmic energy; see [10, 21] for more details. In computations, we employ a cut-off approach to numerically preserve this physical constraint, which is a common strategy in phase-field simulations, see e.g. [35, 50, 57]. This technique enables stable simulations with large parameter ratios.

4.2. Numerical investigation on magnetic damping effects

In this section, we present a three-dimensional numerical example of magnetic damping effects on bubble dynamics. This problem finds its applications in metallurgy processes [55], where injected bubbles serve to stir and homogenize molten metals, with magnetic fields providing a non-intrusive approach to control bubbles' motion. While it has been extensively investigated both experimentally [23, 58, 62] and numerically

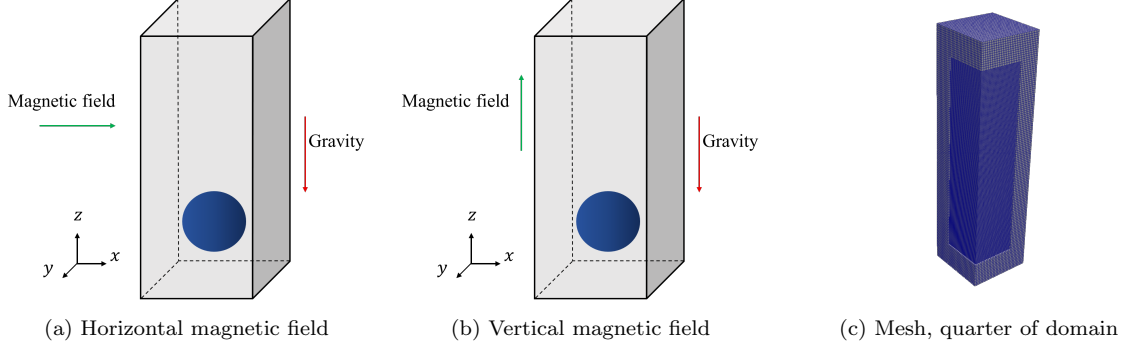


Figure 1: Setup of single rising bubble under magnetic fields.

[64, 65, 67], the test cases we considered here is a generalization of a classical two-phase flow benchmark originally proposed by Hysing et al. [31]. In this benchmark problem a bubble of lighter fluid with radius 0.5 m is centered at (0.5, 0.5, 0.5) m in the domain $\Omega = (0, 1) \text{ m} \times (0, 1) \text{ m} \times (0, 2) \text{ m}$, corresponding to the following initial profile for ϕ ,

$$\phi^0 = \tanh \left(\frac{\sqrt{(x-0.5)^2 + (y-0.5)^2 + (z-0.5)^2} - 0.25}{\sqrt{2} \text{Cn}} \right).$$

The relevant physical parameters are

- densities ($\text{kg} \cdot \text{m}^{-3}$): $\rho_+ = 1000$, $\rho_- = 1$;
- dynamic viscosities ($\text{kg} \cdot \text{m}^{-1} \cdot \text{s}^{-1}$): $\eta_+ = 10$, $\eta_- = 0.1$;
- electrical conductivities ($\text{S} \cdot \text{m}^{-1}$): $\sigma_+ = 1000$, $\sigma_- = 1$;
- surface tension ($\text{N} \cdot \text{m}^{-1}$): $\lambda = 1.96$;
- gravitational acceleration ($\text{m} \cdot \text{s}^{-2}$): $g = 0.98$;
- magnetic fields (T): a horizontal magnetic field $\mathbf{B} = (B_r, 0, 0)^\top$ and a vertical magnetic field $\mathbf{B} = (0, 0, B_r)^\top$, with $B_r = 3, 5$, and 7 .

Our numerical implementation relies on the `deal.II` finite element library [4, 5] with `ParaView` post-processing software (www.paraview.org). And the proposed BDF-2 scheme, initialized via BDF-1, is utilized in simulation. Additionally, we discretize all variables with \mathbb{Q}_1 element and solve the resulting linear systems using the flexible generalized minimum residual (FGMRES) algorithm with preconditioning: block-Jacobi for equations (31) and algebraic multigrid (AMG) for equations (32)-(34), provided by `Trilinos` packages [27].

While adaptive mesh refinement (AMR) techniques lead to a poor mass conservation result [35] and present challenges in designing a desirable refinement strategy, we only adopt a fixed locally refined mesh to resolve interfacial dynamics. Specifically, we set mesh size $h = 2^{-7} \text{ m}$ in subdomain $(0.15, 0.85) \text{ m} \times (0.15, 0.85) \text{ m} \times (0.2, 1.8) \text{ m}$ and $h = 2^{-6} \text{ m}$ elsewhere; see Figure 1c. This configuration generates 1,906,592 cells, resulting in 1,960,255 degrees of freedom per system component. In terms of temporal discretization, we set the final dimensional time $T^* = 3 \text{ s}$ with a fixed time step of $1 \times 10^{-3} \text{ s}$, giving 3,000 total steps. With regard to characteristic quantities, we select $\epsilon = 0.005 \text{ m}$, $L_r = 1 \text{ m}$, $u_r = \sqrt{gL_r}$, $\rho_r = \rho_+$, $\eta_r = \eta_+$, and $\sigma_r = \sigma_+$. All results were obtained in a machine with AMD EPYC 9654 and 768 GB RAM.

The cross-sections of the order parameter ϕ at different dimensional time instants t^* are presented in Figure 2 (in the absence of magnetic fields), Figure 3 (under horizontal magnetic fields), and Figure 4 (under vertical magnetic fields); a comparison of final bubble shape can be found in Figure 5. The corresponding velocity streamlines, visualized via the “Surface LIC” configuration in `ParaView`, are also depicted in these figures. In addition, Figure 6 shows the rise velocity and mass drift, which are defined as

$$\frac{\int_{\phi < 0} u_3 d\mathbf{x}}{\int_{\phi < 0} d\mathbf{x}} \quad \text{and} \quad \int_{\Omega} \phi d\mathbf{x} - \int_{\Omega} \phi^0 d\mathbf{x},$$

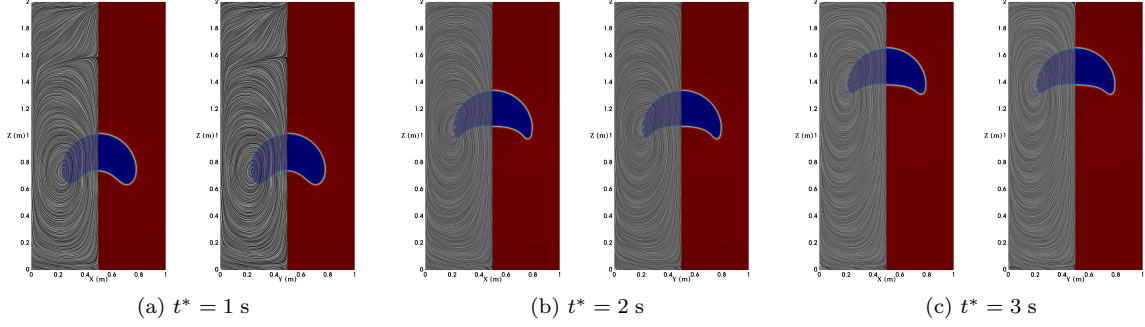


Figure 2: Cross-sections of ϕ_h^n without magnetic fields, with streamline distributions of \mathbf{u}_h^n depicted on the left-hand side.

respectively. For all the reported cases, it is clearly observable that the change in the total mass is of the order $\mathcal{O}(10^{-10})$. This illustrates excellent mass conservation property of our numerical method in practical physical simulations. Moreover, the following conclusions can be drawn:

- **velocity characteristics:** horizontal magnetic fields exert a significant damping effect on the bubble rise velocity. In contrast, vertical fields display a non-monotonic influence. As the magnetic intensity increases, the velocity field becomes increasingly parallel with the magnetic fields, which is clearly demonstrated by the streamline distributions.
- **interface dynamics:** vertical magnetic fields preserve an axisymmetric bubble shape similar to non-magnetic scenarios. Conversely, horizontal magnetic fields give rise to anisotropic deformations, compressing the bubble shape along the field direction. And in all cases, stronger magnetic fields lead to a progressive suppression of bubble motion.

These numerical observations are in qualitative agreement with previous results reported in [64, 65, 67], in turn validating the capacity of our model to capture the magnetic damping effects on bubble dynamics.

5. Concluding remarks

In this paper, we established a mathematical framework to simulate two-phase MHD flows at a magnetic Reynolds number $Rm \ll 1$. Leveraging the low- Rm approximation, we first formulated an underlying sharp-interface system. Subsequently, by means of Onsager’s variational principle, we exploited phase-field methods to characterize the interface and derived a thermodynamically consistent model. This formulation integrates the AGG model of two-phase flows with a generalized Darcy’s law accounting for electromagnetic effects. From a theoretical perspective, we carried out an asymptotic analysis via method of formally matched asymptotic expansions. Provided a scaling law for the mobility from [39], we deduced that the sharp-interface system can be recovered in the vanishing interface thickness limit, which illustrates the robustness of the phase-field approach as an approximated method. Regarding numerical implementation, we proposed an efficient decoupled and linear finite element algorithm based on a dimensionless form of the phase-field model. And using this algorithm, we explored the magnetic damping effects through a single rising bubble benchmark. The observed flow mechanisms were found to be consistent with the results reported in [64, 65, 67], in turn validating the proposed framework.

Although the developed framework is capable of effectively capturing MHD interfacial phenomena, such as magnetic damping effects, our discussions are still relatively circumscribed. We identify several areas for future research. First, it is essential to formulate a general sharp-interface system that incorporates the full pre-Maxwell equations. Of course, taking thermocapillary effects into account is also indispensable, in view of practical industrial applications [64, 66]. Another vital aspect for future investigation lies in the exploration of other MHD phenomena within this framework, for instance, metal pad rolling in multilayer liquid metal systems [28, 29, 69], which further involves moving contact line dynamics. Finally, it is highly desirable to develop structure-preserving numerical schemes for the phase-field model that can preserve fundamental physical properties through convenient formulations.

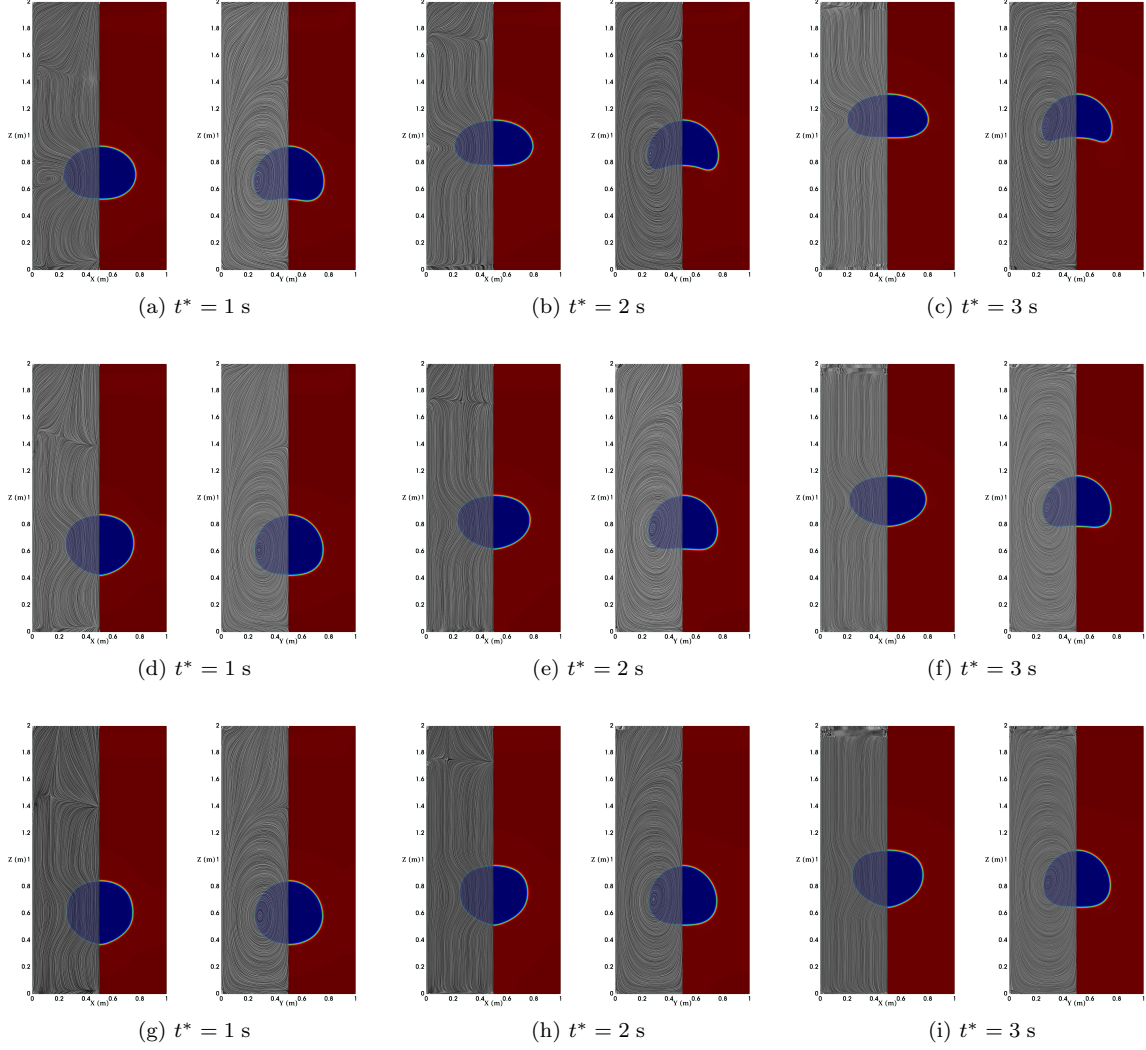


Figure 3: Cross-sections of ϕ_h^n under horizontal magnetic fields, with streamline distributions of \mathbf{u}_h^n depicted on the left-hand side. Top row: $B_r = 3$ T; middle row: $B_r = 5$ T; bottom row: $B_r = 7$ T.

Acknowledgments

Authors want to thank Associate Professor Wenyu Lei (UESTC) for the fruitful discussions on numerical implementations using `deal.II`. The research of M. Li was supported in part by the NSFC 12271082, 62231016. The research of Z. Xia was supported in part by the NSFC 12471371. The research of L. Xu was supported in part by the NSFC 12431015, 62231016.

References

- [1] H. Abels, H. Garcke, and A. Giorgini. Global regularity and asymptotic stabilization for the incompressible Navier-Stokes-Cahn-Hilliard model with unmatched densities. *Math. Ann.*, 389(2):1267–1321, 2024.
- [2] H. Abels, H. Garcke, and G. Grün. Thermodynamically consistent, frame indifferent diffuse interface models for incompressible two-phase flows with different densities. *Math. Models Methods Appl. Sci.*, 22(3):1150013, 40, 2012.
- [3] G. L. Aki, W. Dreyer, J. Giesselmann, and C. Kraus. A quasi-incompressible diffuse interface model with phase transition. *Math. Models Methods Appl. Sci.*, 24(5):827–861, 2014.

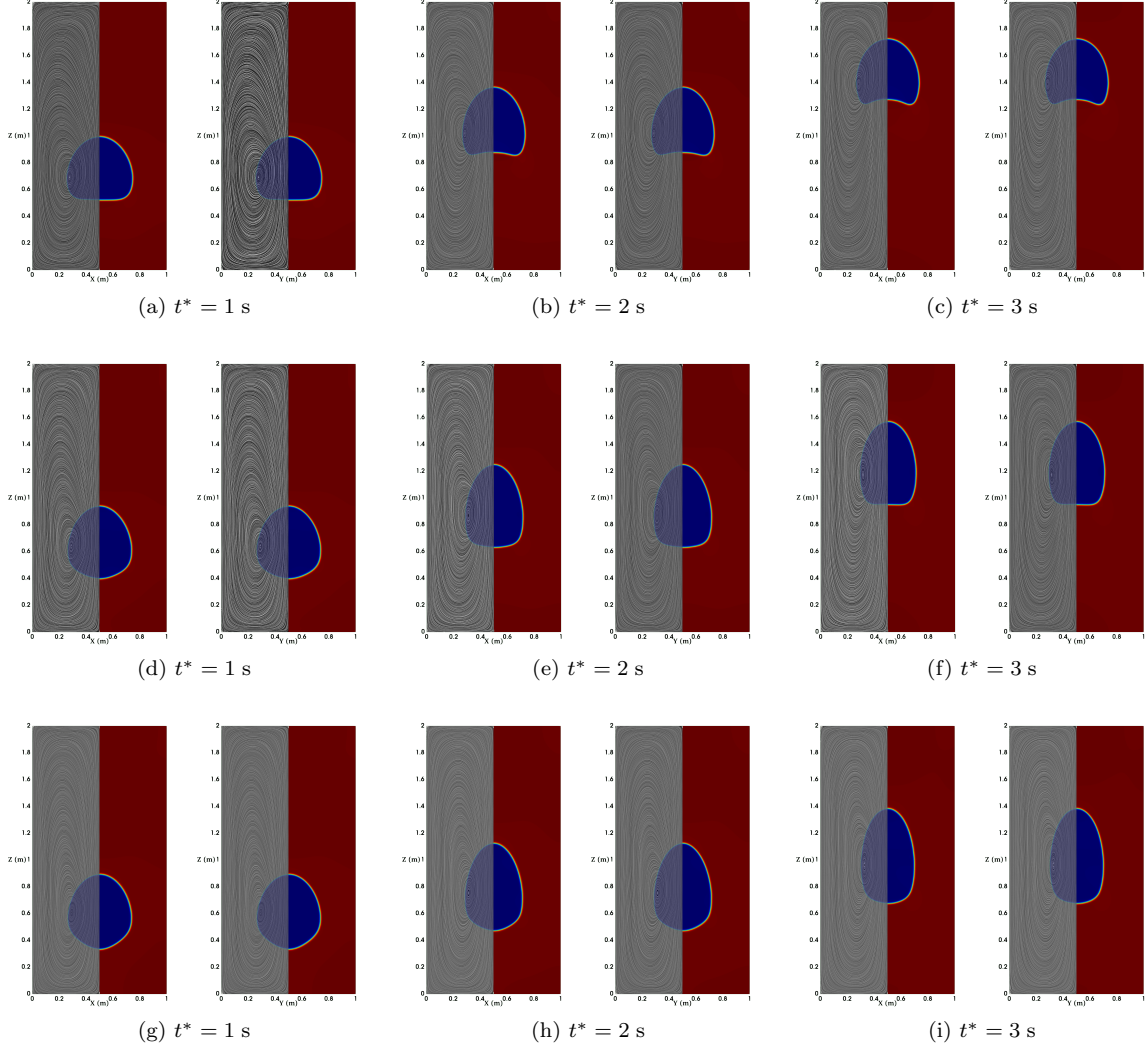


Figure 4: Cross-sections of ϕ_h^n under vertical magnetic fields, with streamline distributions of \mathbf{u}_h^n depicted on the left-hand side. Top row: $B_r = 3$ T; middle row: $B_r = 5$ T; bottom row: $B_r = 7$ T.

- [4] D. Arndt, W. Bangerth, M. Bergbauer, M. Feder, M. Fehling, J. Heinz, T. Heister, L. Heltai, M. Kronbichler, M. Maier, P. Munch, J.-P. Pelteret, B. Turcksin, D. Wells, and S. Zampini. The deal.II library, version 9.5. *J. Numer. Math.*, 31(3):231–246, 2023.
- [5] D. Arndt, W. Bangerth, D. Davydov, T. Heister, L. Heltai, M. Kronbichler, M. Maier, J.-P. Pelteret, B. Turcksin, and D. Wells. The deal.II finite element library: design, features, and insights. *Comput. Math. Appl.*, 81:407–422, 2021.
- [6] J. W. Barrett, H. Garcke, and R. Nürnberg. Parametric finite element approximations of curvature-driven interface evolutions. In A. Bonito and R. H. Nochetto, editors, *Geometric partial differential equations. Part I*, volume 21 of *Handb. Numer. Anal.*, pages 275–423. Elsevier, 2020.
- [7] L. Bañas and A. Prohl. Convergent finite element discretization of the multi-fluid nonstationary incompressible magnetohydrodynamics equations. *Math. Comp.*, 79(272):1957–1999, 2010.
- [8] E. Campillo-Funollet, G. Grün, and F. Klingbeil. On modeling and simulation of electrokinetic phenomena in two-phase flow with general mass densities. *SIAM J. Appl. Math.*, 72(6):1899–1925, 2012.
- [9] C. Chen and X. Yang. Fully-discrete finite element numerical scheme with decoupling structure and energy stability for the Cahn-Hilliard phase-field model of two-phase incompressible flow system with variable density and viscosity. *ESAIM Math. Model. Numer. Anal.*, 55(5):2323–2347, 2021.

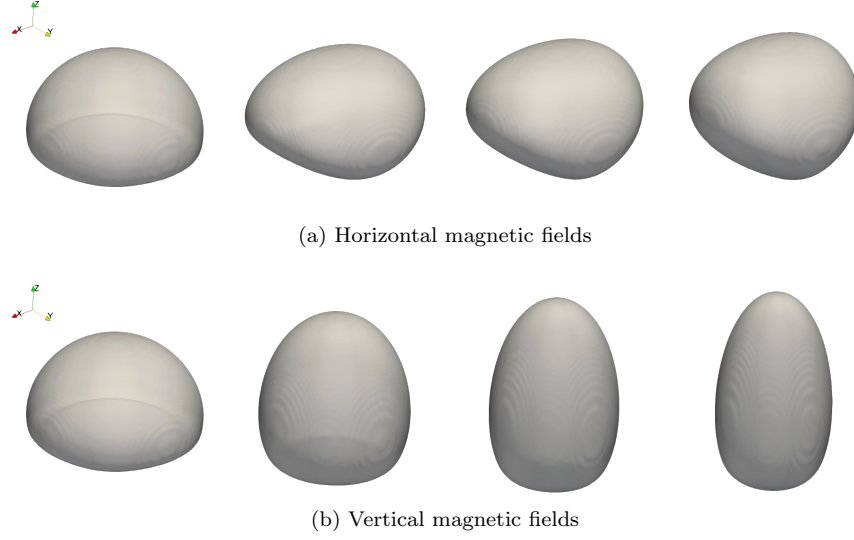


Figure 5: Final bubble shape. Left to right: $B_r = 0, 3, 5$, and 7 T.

- [10] W. Chen, J. Jing, C. Wang, X. Wang, and S. M. Wise. A modified Crank-Nicolson numerical scheme for the Flory-Huggins Cahn-Hilliard model. *Commun. Comput. Phys.*, 31(1):60–93, 2022.
- [11] P. A. Davidson. Magnetohydrodynamics in materials processing. *Annu. Rev. Fluid Mech.*, 31(1):273–300, 1999.
- [12] P. A. Davidson. *Introduction to magnetohydrodynamics*. Cambridge Texts in Applied Mathematics. Cambridge University Press, Cambridge, second edition, 2017.
- [13] A. E. Diegel, C. Wang, X. Wang, and S. M. Wise. Convergence analysis and error estimates for a second order accurate finite element method for the Cahn-Hilliard-Navier-Stokes system. *Numer. Math.*, 137(3):495–534, 2017.
- [14] A. Ern and J.-L. Guermond. *Finite elements II—Galerkin approximation, elliptic and mixed PDEs*, volume 73 of *Texts in Applied Mathematics*. Springer, Cham, 2021.
- [15] X. Feng, Z. Qiao, S. Sun, and X. Wang. An energy-stable smoothed particle hydrodynamics discretization of the Navier-Stokes-Cahn-Hilliard model for incompressible two-phase flows. *J. Comput. Phys.*, 479:Paper No. 111997, 20, 2023.
- [16] M. Flueck, A. Janka, C. Laurent, M. Picasso, J. Rappaz, and G. Steiner. Some mathematical and numerical aspects in aluminum production. *J. Sci. Comput.*, 43(3):313–325, 2010.
- [17] G. Fu and D. Han. A linear second-order in time unconditionally energy stable finite element scheme for a Cahn-Hilliard phase-field model for two-phase incompressible flow of variable densities. *Comput. Methods Appl. Mech. Engrg.*, 387:Paper No. 114186, 21, 2021.
- [18] C. G. Gal, M. Grasselli, and H. Wu. Global weak solutions to a diffuse interface model for incompressible two-phase flows with moving contact lines and different densities. *Arch. Ration. Mech. Anal.*, 234(1):1–56, 2019.
- [19] J.-F. Gerbeau, C. Le Bris, and T. Lelièvre. *Mathematical methods for the magnetohydrodynamics of liquid metals*. Numerical Mathematics and Scientific Computation. Oxford University Press, Oxford, 2006.
- [20] J.-F. Gerbeau, T. Lelièvre, and C. Le Bris. Simulations of MHD flows with moving interfaces. *J. Comput. Phys.*, 184(1):163–191, 2003.
- [21] A. Giorgini, A. Miranville, and R. Temam. Uniqueness and regularity for the Navier-Stokes-Cahn-Hilliard system. *SIAM J. Math. Anal.*, 51(3):2535–2574, 2019.
- [22] Y. Gong, J. Zhao, X. Yang, and Q. Wang. Fully discrete second-order linear schemes for hydrodynamic phase field models of binary viscous fluid flows with variable densities. *SIAM J. Sci. Comput.*, 40(1):B138–B167, 2018.
- [23] H.-Y. Gou, M.-J. Ni, and Z.-H. Yao. Experimental study of a single bubble’s motion in a liquid metal under a horizontal magnetic field. *J. Fluid Mech.*, 988:Paper No. A21, 25, 2024.

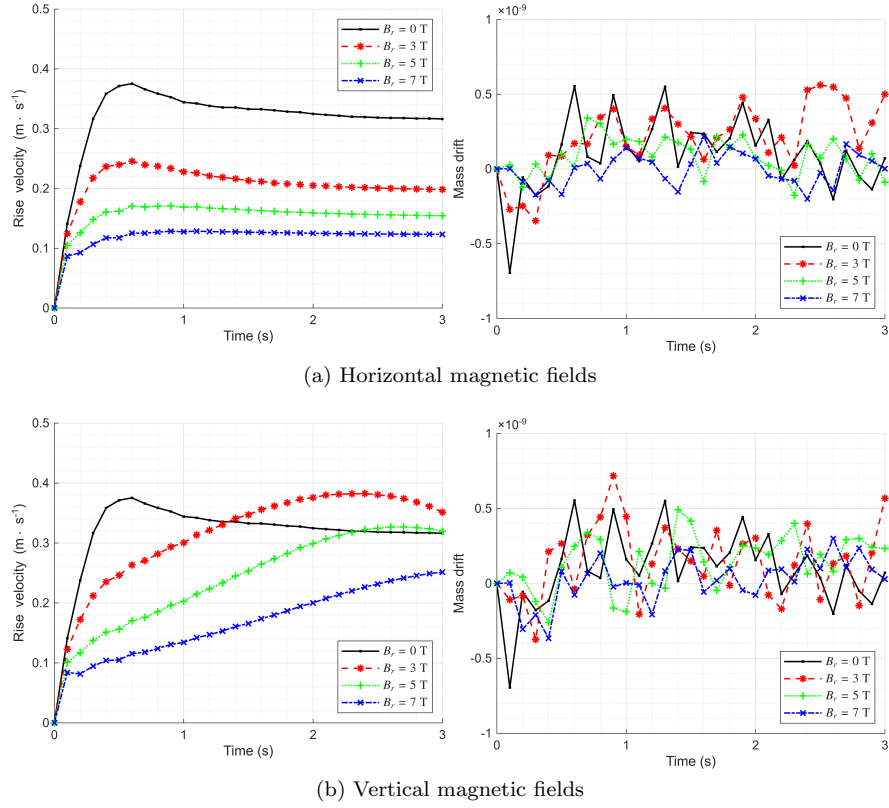


Figure 6: Derived benchmark quantities.

- [24] S. Gross and A. Reusken. *Numerical methods for two-phase incompressible flows*, volume 40 of *Springer Series in Computational Mathematics*. Springer-Verlag, Berlin, 2011.
- [25] G. Grün and S. Metzger. On micro-macro-models for two-phase flow with dilute polymeric solutions—modeling and analysis. *Math. Models Methods Appl. Sci.*, 26(5):823–866, 2016.
- [26] J.-L. Guermond and A. Salgado. A splitting method for incompressible flows with variable density based on a pressure Poisson equation. *J. Comput. Phys.*, 228(8):2834–2846, 2009.
- [27] M. A. Heroux, R. A. Bartlett, V. E. Howle, R. J. Hoekstra, J. J. Hu, T. G. Kolda, R. B. Lehoucq, K. R. Long, R. P. Pawlowski, E. T. Phipps, A. G. Salinger, H. K. Thornquist, R. S. Tuminaro, J. M. Willenbring, A. Williams, and K. S. Stanley. An overview of the Trilinos Project. *ACM Trans. Math. Software*, 31(3):397–423, 2005.
- [28] W. Herreman, C. Nore, J.-L. Guermond, L. Cappanera, N. Weber, and G. M. Horstmann. Perturbation theory for metal pad roll instability in cylindrical reduction cells. *J. Fluid Mech.*, 878:598–646, 2019.
- [29] W. Herreman, L. Wierzbalek, G. M. Horstmann, L. Cappanera, and C. Nore. Stability theory for metal pad roll in cylindrical liquid metal batteries. *J. Fluid Mech.*, 962:Paper No. A6, 37, 2023.
- [30] J. S. Hu, G. Z. Zuo, L. Li, D. H. Zhang, H. L. Bi, Z. B. Ye, J. H. Pan, S. Y. Dai, X. C. Meng, Z. Sun, M. Ono, Y. Hirooka, and D. N. Ruzic. Recent progress in the development of liquid metal plasma facing components for magnetic fusion devices. *Nucl. Mater. Energy*, 41:101776, 2024.
- [31] S. Hysing, S. Turek, D. Kuzmin, N. Parolini, E. Burman, S. Ganesan, and L. Tobiska. Quantitative benchmark computations of two-dimensional bubble dynamics. *Internat. J. Numer. Methods Fluids*, 60(11):1259–1288, 2009.
- [32] M. A. Jaworski, T. K. Gray, M. Antonelli, J. J. Kim, C. Y. Lau, M. B. Lee, M. J. Neumann, W. Xu, and D. N. Ruzic. Thermoelectric Magnetohydrodynamic Stirring of Liquid Metals. *Phys. Rev. Lett.*, 104:094503, 2010.
- [33] K. Jin, P. Kumar, S. Vanka, and B. Thomas. Rise of an argon bubble in liquid steel in the presence of a transverse magnetic field. *Phys. Fluids*, 28(9), 2016.
- [34] D. H. Kelley and T. Weier. Fluid Mechanics of Liquid Metal Batteries. *Appl. Mech. Rev.*, 70(2):020801, 2018.

- [35] M. A. Khanwale, K. Saurabh, M. Ishii, H. Sundar, J. A. Rossmannith, and B. Ganapathysubramanian. A projection-based, semi-implicit time-stepping approach for the Cahn-Hilliard Navier-Stokes equations on adaptive octree meshes. *J. Comput. Phys.*, 475:Paper No. 111874, 35, 2023.
- [36] L. Li, M. Ni, and W. Zheng. A charge-conservative finite element method for inductionless MHD equations. Part I: Convergence. *SIAM J. Sci. Comput.*, 41(4):B796–B815, 2019.
- [37] J. Lowengrub and L. Truskinovsky. Quasi-incompressible Cahn-Hilliard fluids and topological transitions. *R. Soc. Lond. Proc. Ser. A Math. Phys. Eng. Sci.*, 454(1978):2617–2654, 1998.
- [38] D. Lunz and P. D. Howell. Flow of a thin liquid-metal film in a toroidal magnetic field. *J. Fluid Mech.*, 867:835–876, 2019.
- [39] F. Magaletti, F. Picano, M. Chinappi, L. Marino, and C. M. Casciola. The sharp-interface limit of the Cahn-Hilliard/Navier-Stokes model for binary fluids. *J. Fluid Mech.*, 714:95–126, 2013.
- [40] A. Maurya and P. K. Jha. Influence of electromagnetic stirrer position on fluid flow and solidification in continuous casting mold. *Appl. Math. Model.*, 48:736–748, 2017.
- [41] N. Morley, S. Smolentsev, R. Munipalli, M.-J. Ni, D. Gao, and M. Abdou. Progress on the modeling of liquid metal, free surface, MHD flows for fusion liquid walls. *Fusion Eng. Des.*, 72(1):3–34, 2004.
- [42] D. Munger and A. Vincent. A level set approach to simulate magnetohydrodynamic-instabilities in aluminum reduction cells. *J. Comput. Phys.*, 217(2):295–311, 2006.
- [43] T. T. Natarajan and N. El-Kaddah. Finite element analysis of electromagnetic and fluid flow phenomena in rotary electromagnetic stirring of steel. *Appl. Math. Model.*, 28(1):47–61, 2004.
- [44] M.-J. Ni, R. Munipalli, N. B. Morley, P. Huang, and M. A. Abdou. A current density conservative scheme for incompressible MHD flows at a low magnetic Reynolds number. I. On a rectangular collocated grid system. *J. Comput. Phys.*, 227(1):174–204, 2007.
- [45] R. L. Pego. Front migration in the nonlinear Cahn-Hilliard equation. *Proc. Roy. Soc. London Ser. A*, 422(1863):261–278, 1989.
- [46] T. Qian, X.-P. Wang, and P. Sheng. A variational approach to moving contact line hydrodynamics. *J. Fluid Mech.*, 564:333–360, 2006.
- [47] C. Rohde and L. von Wolff. A ternary Cahn-Hilliard-Navier-Stokes model for two-phase flow with precipitation and dissolution. *Math. Models Methods Appl. Sci.*, 31(1):1–35, 2021.
- [48] Y. Safa, M. Flueck, and J. Rappaz. Numerical simulation of thermal problems coupled with magnetohydrodynamic effects in aluminium cell. *Appl. Math. Model.*, 33(3):1479–1492, 2009.
- [49] R. Samulyak, J. Du, J. Glimm, and Z. Xu. A numerical algorithm for MHD of free surface flows at low magnetic Reynolds numbers. *J. Comput. Phys.*, 226(2):1532–1549, 2007.
- [50] J. Shen and X. Yang. Decoupled, energy stable schemes for phase-field models of two-phase incompressible flows. *SIAM J. Numer. Anal.*, 53(1):279–296, 2015.
- [51] J. Shen, X. Yang, and Q. Wang. Mass and volume conservation in phase field models for binary fluids. *Commun. Comput. Phys.*, 13(4):1045–1065, 2013.
- [52] M. Shokrpour Roudbari, G. Simsek, E. H. van Brummelen, and K. G. van der Zee. Diffuse-interface two-phase flow models with different densities: a new quasi-incompressible form and a linear energy-stable method. *Math. Models Methods Appl. Sci.*, 28(4):733–770, 2018.
- [53] S. Siriano, L. Melchiorri, S. Pignatiello, and A. Tassone. A multi-region and a multiphase MHD OpenFOAM solver for fusion reactor analysis. *Fusion Eng. Des.*, 200:114216, 2024.
- [54] M. F. P. ten Eikelder, K. G. van der Zee, I. Akkerman, and D. Schillinger. A unified framework for Navier-Stokes Cahn-Hilliard models with non-matching densities. *Math. Models Methods Appl. Sci.*, 33(1):175–221, 2023.
- [55] B. G. Thomas. Review on Modeling and Simulation of Continuous Casting. *Steel Res. Int.*, 89(1):1700312, 2018.
- [56] A. Tucs, V. Bojarevics, and K. Pericleous. Magnetohydrodynamic stability of large scale liquid metal batteries. *J. Fluid Mech.*, 852:453–483, 2018.

- [57] J. Wang, M. Li, and C. Wang. Efficient finite element schemes for a phase field model of two-phase incompressible flows with different densities. *J. Comput. Phys.*, 518:Paper No. 113331, 28, 2024.
- [58] Z. H. Wang, S. D. Wang, X. Meng, and M. J. Ni. UDV measurements of single bubble rising in a liquid metal Galinstan with a transverse magnetic field. *Int. J. Multiph. Flow*, 94:201–208, 2017.
- [59] X. Xu, Y. Di, and H. Yu. Sharp-interface limits of a phase-field model with a generalized Navier slip boundary condition for moving contact lines. *J. Fluid Mech.*, 849:805–833, 2018.
- [60] J. Yang, I. C. Christov, and S. Dong. Phase field modeling and numerical algorithm for two-phase dielectric fluid flows. *J. Comput. Phys.*, 514:Paper No. 113228, 36, 2024.
- [61] Z. Yang and S. Dong. An unconditionally energy-stable scheme based on an implicit auxiliary energy variable for incompressible two-phase flows with different densities involving only precomputable coefficient matrices. *J. Comput. Phys.*, 393:229–257, 2019.
- [62] C. Zhang, S. Eckert, and G. Gerbeth. Experimental study of single bubble motion in a liquid metal column exposed to a DC magnetic field. *Int. J. Multiph. Flow*, 31(7):824–842, 2005.
- [63] J. Zhang, L. Luo, and X. Wang. A fully-decoupled second-order-in-time and unconditionally energy stable scheme for the Cahn-Hilliard-Navier-Stokes equations with variable density. *J. Comput. Phys.*, 532:Paper No. 113943, 22, 2025.
- [64] J. Zhang and M.-J. Ni. Direct simulation of multi-phase MHD flows on an unstructured Cartesian adaptive system. *J. Comput. Phys.*, 270:345–365, 2014.
- [65] J. Zhang and M.-J. Ni. Direct simulation of single bubble motion under vertical magnetic field: Paths and wakes. *Phys. Fluids*, 26(10), 2014.
- [66] J. Zhang and M.-J. Ni. Direct numerical simulations of incompressible multiphase magnetohydrodynamics with phase change. *J. Comput. Phys.*, 375:717–746, 2018.
- [67] J. Zhang, M.-J. Ni, and R. Moreau. Rising motion of a single bubble through a liquid metal in the presence of a horizontal magnetic field. *Phys. Fluids*, 28(3):032101, 2016.
- [68] J. Zhao and D. Han. Second-order decoupled energy-stable schemes for Cahn-Hilliard-Navier-Stokes equations. *J. Comput. Phys.*, 443:Paper No. 110536, 30, 2021.
- [69] O. Zikanov. Metal pad instabilities in liquid metal batteries. *Phys. Rev. E*, 92(6):063021, 8, 2015.